*DOI:*
10.1002/mrm.27448

*Document Version*
Peer reviewed version


# Rigid Motion Corrected Magnetic Resonance Fingerprinting

| | |
|---|---|
| Journal: | *Magnetic Resonance in Medicine* |
| Manuscript ID | MRM-18-18696.R3 |
| Wiley - Manuscript type: | Full Paper |
| Date Submitted by the Author: | 06-Jun-2018 |
| Complete List of Authors: | Lima da Cruz, Gastão; King's College London, Imaging Sciences & Biomedical Engineering<br>Jaubert, Olivier<br>Schneider, Torben; Philips Healthcare United Kingdom,<br>Botnar, Rene; King's College London, Imaging Sciences Division;<br>Prieto, Claudia; King's College London, Interdisciplinary Medical Imaging Group |
| Research Type: | Relaxation techniques < Technique Development < Technical Research |
| Research Focus: | Normal < Anatomy < Brain < Neurological |
| | |

# Rigid Motion Corrected Magnetic Resonance Fingerprinting

G. Cruz[1], O. Jaubert[1], T. Schneider[2], R. M. Botnar[1,3], C. Prieto[1,3]

[1]King's College London,
School of Biomedical Engineering and Imaging Sciences,
London, United Kingdom.

[2]Philips Healthcare,
Guilford, United Kingdom.

[3]Pontificia Universidad Católica de Chile,
Escuela de Ingeniería,
Santiago, Chile.



Short Title: Rigid motion corrected MRF
Submitted as Full Paper to Magnetic Resonance in Medicine.
Word count: ~4335

**Corresponding author:**

Gastao Cruz
School of Biomedical Engineering
and Imaging Sciences,
3rd Floor, Lambeth Wing,
St Thomas' Hospital,
London, SE1 7EH, United Kingdom.
E-mail: gastao.cruz@kcl.ac.uk

## Abstract

**Purpose:** Develop a method for rigid body motion corrected Magnetic Resonance Fingerprinting (MRF).

**Methods:** MRF has shown some robustness to abrupt motion towards the end of the acquisition. Here, we study the effects of different types of rigid body motion during the acquisition on MRF and propose a novel approach to correct for this motion. The proposed method (MC-MRF) follows four steps: 1) sliding window reconstruction is performed to produce high quality auxiliary dynamic images; 2) rotation and translation motion is estimated from the dynamic images via image registration; 3) estimated motion is used to correct acquired k-space data with corresponding rotations and phase-shifts; 4) motion corrected data is reconstructed with low rank inversion. MC-MRF was validated in a standard $T_1/T_2$ phantom and 2D *in-vivo* brain acquisitions in seven healthy subjects. Additionally, the effect of through-plane motion in 2D MC-MRF was investigated.

**Results:** Simulation results show that motion in MRF can introduce artefacts in $T_1$ and $T_2$ maps, depending when it occurs. MC-MRF improved parametric map quality in all phantom and *in-vivo* experiments with in-plane motion, comparable to the no motion ground truth. Reduced parametric map quality even after motion correction was observed for acquisitions with through-plane motion, particularly for smaller structures in $T_2$ maps.

**Conclusion:** Here, a novel method for motion correction in MRF (MC-MRF) is proposed, which improves parametric map quality and accuracy in comparison to no motion correction approaches. Future work will include validation of 3D MC-MRF to enable also through-plane motion correction.

**Keywords**: MR fingerprinting; rigid motion correction; low rank.

# Introduction

Magnetic Resonance Fingerprinting (MRF) is a novel relaxometry approach based on continuous sampling of the transient steady state magnetization evolution (1). In MRF, sequence parameters, predominantly flip angle (FA) and repetition time (TR), are varied to explore different magnetization states. Moreover, undersampled trajectories are employed to sample each combination of sequence parameters (time-points) at high temporal resolution. Under these conditions, each unique tissue parameter (e.g. $T_1/T_2$) combination is expected to produce a unique signal evolution (fingerprint) that can be simulated using Bloch equations or Extended Phase Graphs (2, 3). The set of simulated signal evolutions (dictionary) can be matched to the measured fingerprints to simultaneously determine tissue parameters like $T_1$, $T_2$ and $M_0$. Incoherent spatial and temporal aliasing of the sampled magnetization time-points (due to undersampling) is typically achieved with non-Cartesian trajectories to minimize potential bias in dictionary matching step.

Considerable efforts have focused on improving various parts of the MRF approach; among them improving the MRF reconstruction to achieve further scan acceleration. A multi-scale MRF reconstruction approach was introduced to reduce the number of measurements by a factor of 3 relative to the original MRF work (4). Integration of MRF with simultaneous multi-slice with an acceleration factor of two has also been achieved (5). Sliding window and soft-weighted reconstructions have also been proposed to share data between time-points, improving measurement precision and accuracy (6, 7). Recently, general formulations using low rank approximations have been introduced for MRF (8-13). Low rank models have been previously introduced in other MR applications to enable higher acceleration factors (14-17). Fingerprints from different tissues within the dictionary are highly correlated and methods like the Singular Value Decomposition (SVD) can be used to temporally compress the fingerprints (8). It has been shown that reconstructions in the compressed domain are faster and better posed. A low rank projection method operating in k-space was also proposed, reducing aliasing artefacts (9). The low rank constraint was directly incorporated into the encoding operator and formulated as a least squares problem in (10), improving parametric map accuracy. A similar approach was taken in (11), but the reconstruction was further regularized by the best dictionary matches using the alternating direction method of multipliers (18).

MRF was originally introduced for 2D brain acquisitions (1). Recent works have explored further applications, such as abdominal (19) and cardiac (20) MRF, where physiological

motion is a well-known problem. Although the original study (1) demonstrated robustness to abrupt motion towards the end of the acquisition, the impact of motion during the MRF acquisition has not been fully investigated. In conventional MRI, several frameworks have been developed to estimate and correct for motion during the acquisition; particularly for brain applications methods have been proposed that estimate the motion from the data itself (21, 22). Some preliminary works have observed sensitivity to motion during the acquisition in MRF (23-27). Initial approaches for motion compensation/correction in MRF have also been investigated. In (23), MRF motion correction is achieved by iteratively identifying corrupted time-points, estimating motion and enforcing data consistency. The method in (24) used a sliding window reconstruction, followed by image registration to align the time-point images before dictionary matching. In (25) a similar approach was followed; however, the estimated motion from image registration was used to directly correct the k-space data and produce a motion corrected MRF reconstruction. Results from (26) introduced gating in MRF as a form of motion compensation. Another approach that has been proposed to minimise motion artefacts is to modify the sampling order such that motion produces incoherent artefacts (27).

Low rank approaches reconstruct compressed images from all acquired data, as mentioned above. In the presence of motion, these reconstructions may introduce motion artefacts (e.g. ghosting and blurring) in addition to quantitative errors due to misregistration between time-point images. In this work simulations were used to investigate the effect of different types of motion in MRF. A novel approach for rigid motion corrected MRF using a low rank reconstruction (MC-MRF) is proposed. With MC-MRF, rigid body motion is estimated from an auxiliary sliding window reconstruction. The estimated motion is used to correct k-space, followed by a motion corrected low rank reconstruction. We investigated the proposed approach to correct for 2D in-plane motion in a standardized $T_1/T_2$ phantom and in brain acquisitions *in-vivo*. Additionally, we investigated the effect of through-plane motion in 2D MC-MRF.

# Methods

The presence of motion during MRF causes a spatial mismatch between time-point images and causes errors in the estimated maps as well as ghosting and blurring artefacts if the data is reconstructed with some data sharing techniques (e.g. low rank approximation). To address

this problem, in this work we propose a novel motion corrected MRF reconstruction (MC-MRF). With the proposed MC-MRF approach, motion is first estimated and corrected in k-space prior to a low rank reconstruction. The proposed method can be divided in four steps: 1) iterative SENSE (28) sliding window reconstruction; 2) rigid body image registration; 3) k-space motion correction; and 4) low rank reconstruction (10). A diagram of the proposed method is shown in Figure 1. Examples for time-point images without motion correction and image outputs for steps 1), 2) and 4) of the proposed approach are shown in Supporting Information Figure S1.

## Sliding window reconstruction: intermediate images

MRF typically uses highly accelerated image acquisition, where individual time-point images exhibit severe reconstruction artefacts that can compromise image registration and therefore motion estimation accuracy. Here, an intermediate sliding window reconstruction is used to reduce aliasing artefacts at the expense of temporal resolution. Intermediate images $\hat{\boldsymbol{I}}_t$ are reconstructed with iterative SENSE:

$$\hat{\boldsymbol{I}}_t = arg\ min_{\boldsymbol{I}_t} \|(\boldsymbol{AFCI}_t - \boldsymbol{K_t})\|_2^2 \quad [1]$$

where $\boldsymbol{A}$ is the sampling operator, $\boldsymbol{F}$ is the Fourier transform, $\boldsymbol{C}$ are the coil sensitivities and $\boldsymbol{K_t}$ is the subset of k-space of a sliding window around time-point *t*. Some motion artefacts may be introduced into $\hat{\boldsymbol{I}}_t$, depending on the motion velocity and the size of the sliding window. However, a considerable reduction of aliasing artefacts is expected.

## Rigid body image registration

Rigid image registration is applied to the reconstructed intermediate images to estimate translational and rotational motion from each intermediate image to a reference intermediate image. Due to the varying contrast of the intermediate images, registration is performed using mutual information as similarity measure. To reduce motion estimation errors, image registration is repeated using different reference intermediate images. Estimated motion is taken as the mean of centred motion estimation from each reference.

## k-Space motion correction

The estimated rigid body motion is used to correct the acquired k-space data $\boldsymbol{K}$, producing the motion corrected $\boldsymbol{K'}$. In the presence of rigid motion, the relationship between $\boldsymbol{K}$ and $\boldsymbol{K'}$ is given by:

$$\boldsymbol{K}(\boldsymbol{k_r}) = \boldsymbol{K'}(\boldsymbol{k_r'})\frac{e^{2\pi i(\boldsymbol{k_r}.\boldsymbol{t})}}{|\det(\boldsymbol{A})|} \quad [2]$$

where the matrix $\boldsymbol{A}$ captures the rigid motion, $\boldsymbol{t}$ is the translational component of $\boldsymbol{A}$ and $\boldsymbol{k_r}^{(\prime)}$ are the k-space coordinates before (after) motion, which are related by $\boldsymbol{k_r'} = \boldsymbol{A}^{-T}\boldsymbol{k_r}$.

## Low rank reconstruction

The motion corrected k-space $\boldsymbol{K'}$ is reconstructed using a low rank inversion method (10, 11). Dictionaries commonly used in MRF are highly compressible along the temporal dimension (8). A singular value decomposition (SVD) of the dictionary reveals the first R singular vectors $\boldsymbol{U_R}$ (the left singular vectors of the SVD, truncated to rank R) which are incorporated into the encoding operator of the low rank reconstruction:

$$\hat{\boldsymbol{I}} = \boldsymbol{arg\ min_I}\ \|\boldsymbol{AU_RFCI} - \boldsymbol{K'}\|_2^2 \quad [3]$$

where $\boldsymbol{I}$ are the singular value images, related to the time-point images $\boldsymbol{I'}$ by $\boldsymbol{I} = \boldsymbol{U_R^H I'}$. Every singular image is a linear combination of data from (potentially) every time-point. Thus, if motion is not accounted for, this reconstruction will create typical motion artefacts (e.g. ghosting and blurring), in addition to misregistration between time-points images. Here, k-space is motion corrected before low rank reconstruction, eliminating these issues.

## Experiments

The effects of motion in MRF and the proposed motion correction approach were validated in simulations and a phantom moved continuously by hand. The proposed approach was evaluated with *in-vivo* 2D brain scans in the presence of in-plane, through-plane motion and no motion.

Phantom and *in-vivo* brain data was acquired on a 1.5T Ingenia MR system (Philips, Best, The Netherlands) using a 12-element head coil. The study was approved by the institutional review board and written informed consent was obtained from all subjects according to institutional guidelines.

### Simulations

A digital phantom modelled after a brain scan with realistic $T_1$, $T_2$ and $M_0$ values was used to evaluate the effects of motion in MRF. Acquisition was performed with similar parameters to Jiang et. al. (29) using the same modifications as for the *in-vivo* acquisitions, described below. Three motion simulations were performed by modifying the acquired motion free k-space: 1) 2D abrupt rigid motion occurring at time-point #250 (out of 1750 time-points, towards beginning of the acquisition); 2) 2D abrupt rigid motion occurring at time-point #1500 (out of 1750 time-points, towards end of the acquisition); 3) 2D continuous sinusoidally varying rigid motion. Simulations 1) and 2) used motion amplitudes of $T_x$ = 8 pixels (left-right translation), $T_y$ = 2 pixels (anterior-posterior translation), R = 12º (in-plane rotation). Simulation 3) used motion amplitudes of $T_x$ = 8 pixels, $T_y$ = 2 pixels, R = 24º. The proposed MC-MRF was compared with an Image Based Motion Correction (IBMC) similar to the approach proposed in (24). In IBMC time-point images are reconstructed using sliding window reconstruction, these images are then registered to a common motion state and summed before performing dictionary matching. Here IBMC was implemented considering the first time-point of the sequence as the reference for motion alignment.

### Data acquisition

2D single slice acquisitions were performed on a standardized $T_1/T_2$ phantom (30) and in seven healthy subjects. A similar protocol to (29) was used with FA varying from 0 to 70 degrees; however, with the following differences: FA pattern was slightly modified (Figure

1), constant TR and golden radial trajectory (31) were used. Relevant acquisition parameters are as follows: gradient echo readout, fixed TE/TR = 1.23/4.3 ms, 1750 time-points, 2x2 $mm^2$ in-plane resolution, 10 mm slice thickness, 320x320 $mm^2$ FOV, transverse slice, one golden radial line per time-point, 160 points per radial spoke. As in (29), an inversion recovery (IR) pulse was applied before the beginning of the acquisition. In the phantom experiment, the phantom was continuously moved by hand in the direction perpendicular to the table throughout the acquisition (left-right direction in the corresponding field-of-view). For the brain acquisitions, subjects were instructed for three scans: 1) no head motion, 2) continuous (mostly) in-plane motion (yaw), 3) continuous (mostly) through-plane motion (roll).

## Image Reconstruction

The proposed MC-MRF method was implemented off-line in MATLAB (Mathworks, Natick, Massachusetts, USA). Coil sensitivity maps were estimated from the data itself using ESPIRiT (32), density compensation functions were computed via Voronoi diagrams (33) and non-uniform Fourier transform based on (34) was used. All reconstructions were solved with the Conjugate Gradient method, with maximum number of iterations set to 15 (chosen to naturally regularize the solution). The intermediate sliding window reconstruction used a window of 50 time-points (corresponding to a temporal window of ~200 ms). The number of time-points per window used was determined by inspecting the image quality of several sliding window reconstructions in simulations. This amount of data sharing minimizes aliasing artefacts (which may compromise motion estimation) while maintaining sufficient temporal resolution for head motion estimation. Image registration was performed with MATLAB's image processing toolbox using normalized mutual information as a metric and a gradient descent optimizer. Motion was estimated by registering each intermediate image towards a given reference. To minimize motion estimation errors due to varying signal intensity throughout the MRF acquisition, the registration was repeated multiple times using different intermediate images as reference. Registrations with different references were performed in parallel. The set of reference images was given by $1{:}100{:}N_t$, where $N_t$ is the total number of time-points. The distance of 100 intermediate images was found empirically adequate to minimise motion estimation errors. Motion parameters were estimated by registration to each reference intermediate image. Following, each estimated motion parameter was centred by subtracting its' mean, putting all the estimated parameters in a common frame of reference. Finally, the estimated motion was taken as the average of the

centred motions obtained from the registration to the different references. Translational and rotational motions were corrected applying the corresponding phase-shifts and k-space rotations as described in Eq. 2. The low rank approximation was experimentally determined to have a rank R = 10. The proposed method took approximately 120 minutes (approximately 90 minutes for the sliding window reconstruction, 20 minutes for rigid registration and 10 minutes for low rank reconstruction) on a Linux workstation with 12 Intel Xeon X5675 (3.07 GHz) and 200 GB RAM. Low rank reconstruction, with the same parameters that described before, was also employed to reconstruct data without motion correction for both the motion corrupted and the motion-free acquisitions. Data and MATLAB code of the proposed approach is available at https://kclcvmimaging.wordpress.com/downloads/.

### Dictionary and pattern recognition

The MRF dictionaries were simulated using the Extended Phase Graph (EPG) formalism (2, 3), based on code available in (3). Slice profile correction was employed similar to (35), however no $B_1$ correction was used. Template matching between fingerprints and dictionary were performed using the inner product as in (29). Separate dictionaries were used for the phantom and brain datasets based on the expected tissue range. For the phantom data, $T_1 \in$ [0:30:200, 200:10:600, 600:20:1200, 1200:30:1600] ms, $T_2 \in$ [0:2:70, 70:10:120, 120:5:270] ms; for the brain data, $T_1 \in$ [0:10:800, 800:40:1400, 1400:300:6000] ms, $T_2 \in$ [0:5:100, 100:10:500, 500:50:1000, 1000:300:2600] ms. For the slice profile correction, the slice was discretized into 50 points along the frequency dimension.

## Results

### Simulations

$T_1$, $T_2$ and $M_0$ maps from MRF reconstruction without motion correction, with image based motion correction (IBMC) and with the proposed MC-MRF are shown in Figures 2, 3 and 4 for the three different types of rigid motion simulated, respectively: 1) 2D abrupt motion at time-point #250 (towards the beginning of the acquisition); 2) 2D abrupt motion at time-point #1500 (towards the end of the acquisition); 3) 2D sinusoidally varying motion. In the first case (Figure 2), abrupt motion occurs during high encoding of $T_1$ (close to the IR pulse) and affects primarily the $T_1$ map. In the second case (Figure 3), abrupt motion occurs near high

encoding of $T_2$ (high flip angle) and has corresponding effects in $T_2$. In the third case (Figure 4), sinusoidal motion affects all time-points and corresponding blurring and ghosting artefacts appear in both $T_1$ and $T_2$ maps. Motion artefacts in $M_0$ appear more correlated with motion artefacts in $T_2$ than in $T_1$. With MC-MRF, motion artefacts were virtually eliminated in comparison to the motion-free gold standard, however a slight reduction in resolution was also observed. Rotational motion disturbs the quasi-uniform golden angle distribution, opening gaps in k-space. This effect makes the following low rank reconstruction more ill-conditioned and can produce residual artefacts. With the IBMC, improvements in the parametric maps were also achieved; however residual blurring artefacts were also present, leading to a further decrease in apparent resolution and increase in apparent SNR. This is due to interpolation effects, residual uncorrected motion within each sliding window and residual errors in motion estimation.

Corresponding estimated translation and rotation motion for IBMC and MC-MRF are shown in Supporting Information Figures S2, S3 and S4 for the three different types of motion, respectively. IBMC produced motion estimates similar to MC-MRF, albeit with slightly more errors. This is due to IBMC estimating motion from a single reference image registration, as opposed to using multiple references as in MC-MRF. Good accuracy was generally achieved with MC-MRF, however small errors in motion estimated were observed around time-points of high velocity motion (abrupt discontinuities). Indeed, since MC-MRF estimates motion from intermediate images with a temporal resolution of ~200 ms, it fails to capture abrupt motion in the order of the TR (i.e. ~4 ms).

## Phantom acquisition

Parametric maps for the phantom experiment are shown in Figure 5 (top). Considerable motion artefacts propagate into the parametric maps without motion correction. With the proposed MC-MRF approach, the motion artefacts are virtually eliminated. Corresponding plots for $T_1$ and $T_2$ in comparison to gold standard values (30) are show in Figure 5 (bottom). A loss in precision and accuracy occurs without motion correction; improvements in both these metrics are achieved with the proposed MC-MRF motion correction.

## In-vivo brain acquisitions

Selected time-point images with and without in-plane motion correction are shown in Supporting Information Figure S5, for two subjects 1 and 2. Blurring and ghosting artefacts (in addition to misregistration) are visible when no motion correction is used; conversely both these effects are minimized with the proposed MC-MRF approach. $T_1$, $T_2$ and $M_0$ maps are shown for four representative subjects in Figures 6 and 7. Results without motion correction have ghosting and blurring artefacts, obscuring several brain structures. Motion correction improves parametric maps to a similar quality of the case without motion. The estimated in-plane motion amplitudes for rotation, left-right translation and anterior-posterior translation in the format [minimum, average, maximum] were R = [5.6, 11.1, 18.3] °, $T_x$ = [5.2, 9.3, 19.4] mm and $T_y$ = [0.4, 1.1, 1.8] mm, respectively. The corresponding estimated amplitudes for the through-plane experiments were R = [3.1, 9.3 22.1] °, $T_x$ = [8.7, 17.1, 32.2] mm and $T_y$ = [0.6, 1.8, 4.4] mm, respectively. Subject 1 had the minimum estimated motion amplitudes, whereas subject 4 had the maximum estimated motion amplitudes. The estimated in-plane motion plots in Supporting Information Figure S6 capture the continuous cyclical motion performed by the subjects in Figures 6 and 7.

$T_1$, $T_2$ and $M_0$ maps for the case of through-plane motion are shown for the same four representative subjects in Figures 8 and 9. Again, motion artefacts are present without motion correction. The proposed MC-MRF corrects for some of this motion however considerable artefacts remain after motion correction. These residual artefacts from through-plane motion appear predominantly on the left and right sides of the brain (where maximum through-plane rotation occurs) and have a stronger impact on the $T_2$ maps.

$T_1$ and $T_2$ values for several regions on interest (denoted in Figure 7) are shown in Table 1. $T_1$ values agreed with literature, however $T_2$ values were underestimated for white and grey matter. An additional reduction in observed $T_2$ occurred for cases of through-plane. Parametric values for MC-MRF in the presence of in-plane motion were comparable with the case of no motion; considerably higher standard deviation was observed for the cases of through-plane motion.

## Discussion

A novel method for rigid body motion correction in magnetic resonance fingerprinting was proposed and validated in simulations, a standardized phantom and brain data of healthy

subjects. The proposed approach estimates motion from an intermediate sliding window reconstruction (via image registration) and corrects k-space before a low rank (motion corrected) reconstruction. The framework does not require additional training data and is suitable for accelerated MRF due to the low rank reconstruction. The proposed motion correction method successfully improved parametric maps to a comparable degree to that of no motion for in-plane motion. As expected, residual errors for through-plane motion remained after motion correction, especially in $T_2$ maps.

Simulations show that motion in MRF can affect both $T_1$ and $T_2$ maps, depending when it happens in the acquisition. As the $T_1/T_2$ encoding power varies during the acquisition, motion at different time-points will corrupt the parametric maps differently. Most MRF sequences rely on an initial inversion recovery pulse to encode $T_1$; consequently, motion towards the beginning of the acquisition affects primarily the $T_1$ map. $T_2$ encoding in MRF is generally achieved with spin and stimulated echoes (proportional to $sin^2(FA/2)$ and $sin(FA)$, respectively); consequently time-points associated with echo creation are more likely to affect the $T_2$ map. Motion will affect misregistration between time-points and introduces motion artefacts if the time-point images are reconstructed from k-space data acquired at multiple motion states (e.g. low rank approximation). Misregistration will cause each pixel's tissue to change during the acquisition, effectively making $T_1$ and $T_2$ vary with time. Consequently, misregistration will cause the most errors in the border between tissues where the fingerprint will oscillate between different $T_1/T_2$ values during the acquisition. This bias can affect the template matching step in MRF, leading to a mismatch in the dictionary. Motion artefacts are generally split into blurring and ghosting. Blurring artefacts will give pixels a mix of signal from different tissues. The fingerprint will correspond to a combination of different $T_1/T_2$, similar to a partial volume problem. Ghosting artefacts behave like undersampling artefacts. Temporally, these artefacts are also expected to be noise-like; in the presence of considerable artefacts the fingerprint template match may also fail due to excessive noise.

The proposed MC-MRF was compared with an alternative Image Based Motion Correction (IBMC) in simulations. Parametric maps obtained with IBMC achieved comparable quality to MC-MRF, however IBMC suffered from residual blurring artefacts. At higher acceleration factors, IBMC is expected to produce more aliasing artefacts than MC-MRF. Additionally, if the motion approaches the temporal resolution of the sliding window, residual motion artefacts will propagate into the parametric maps of the IBMC, whereas MC-MRF can correct for motion within the sliding window temporal resolution. A comparison between alternative

strategies for MRF motion correction will be of interest in future work.

For the in-plane *in-vivo* acquisitions MC-MRF provides $T_1$ and $T_2$ white and grey matter values comparable to those obtained from a motionless scan. White and grey matter $T_1$ values were in good agreement with those reported in literature, however $T_2$ values were underestimated. Errors in $T_2$ with respect to literature values were also observed for the no motion acquisitions. Reduced acquisition time led to a reduction of $T_2$ encoding with the current flip angle pattern. Different flip angles patterns that have been shown to be more sensitive to $T_2$ (36) in short acquisition times will be investigated in future work. Here, $B_1$ was not corrected for, which could also lead to errors in $T_2$.

One of the main limitations of the proposed study is its validation in 2D acquisitions, which cannot account for through-plane motion. Results showed that considerable errors remain, especially underestimation of $T_2$, even after employing the proposed MC-MRF to correct for in-plane motion. As different tissues enter and leave the slice, the effective $T_1/T_2$ would be described by a time varying partial volume model. Additionally, as a given tissue moves within the slice it will experience a different $B_1$ phase and amplitude, altering the magnetization history of that tissue. This effect compromises the fingerprint and consequently the template matching. If through-plane motion could be estimated (in relation to measured in-plane motion perhaps), the effect could be corrected by modelling a temporally varying $B_1$ for each spatial location along the slice profile, although it would be computationally expensive. Prospective motion correction could also be used, although other challenges would have to be considered (37). A slice thickness of 10 mm was employed in these experiments to avoid low SNR and to help reduce accidental through-plane motion during in-plane motion experiments. This way, the effects of in-plane and through-plane motion in MRF could be better separated. Future work will consider higher in-plane and through-plane resolutions.

The natural solution for through-plane motion will generally be 3D acquisitions. 3D radial trajectories will be considered (38, 39) to extend the proposed approach. Adequate temporal resolution for the sliding window reconstruction may be a challenge in 3D. In this case, spatial resolution of the sliding window may be reduced or additional regularization may be employed, e.g. Compressed Sensing (40). Additionally, the FOV and/or the TR may need to be reduced. Another limitation of the current work is the temporal resolution of the estimated motion (~200 ms). This resolution is reasonable for head motion or even respiratory motion, but would not be sufficient for faster motion (e.g. cardiac). Alternatively, motion estimation

could be achieved via autofocus (41), potentially achieving a temporal resolution of the order of the TR.

The proposed method only corrects for rigid body motion. Motion correction becomes more challenging as the motion amplitude increases due to possible motion estimation inaccuracies, larger k-space gaps and possibly higher degree of through-plane motion. Expanding the motion correction to more complete models (affine and non-linear) is also of interest in future work. While extension to affine motion correction would be straightforward (using Eq.2), general elastic motion would require more complex solutions such as a motion compensated reconstruction (42) or localized autofocus (43). Finally, the current suboptimal implementation of the proposed framework features slow reconstruction times. This can be improved by reconstructing only a subset of sliding window time-points for motion estimation (with adequate temporal resolution) and/or by reconstructing lower spatial resolution images (which should be sufficient for rigid motion estimation, but may be not be the case for more complex models such as affine or elastic motion).

Future work should incorporate effects missing in the current model, such as $B_1$ inhomogeneity (44) or magnetization transfer effects (45). $B_0$, in addition to both transmit and receive $B_1$ fields can vary in the presence of motion and may need to be accounted in the dictionary simulation. Extension of the current method to 3D MRF (46) is desirable; through-plane motion will be eliminated and motion correction will be more relevant due to the increased scan time. Finally, more complex motion models will be required if the method is to be considered for abdominal or cardiac MRF.



## Conclusion

A novel method for rigid body motion correction in magnetic resonance fingerprinting has been proposed and validated *in-vivo* for 2D acquisitions. For in-plane motion, the proposed motion correction approach produces similar $T_1$ and $T_2$ maps to the case of no motion; however residual errors exist in the case of through-plane motion, particularly for $T_2$.

## Acknowledgments

The authors acknowledge financial support from: (1) EPSRC: EPSRC EP/P001009/, (2)

FONDECYT: 1161055, (3) Wellcome EPSRC Centre for Medical Engineering (NS/A000049/1), (4) the Department of Health via the National Institute for Health Research (NIHR) comprehensive Biomedical Research Centre award to Guy's & St Thomas' NHS Foundation Trust in partnership with King's College London and King's College Hospital NHS Foundation Trust. The views expressed are those of the authors and not necessarily those of the NHS, the NIHR or the Department of Health.

# Figure captions:

Figure 1. Top: plot of the flip angle pattern used for all experiments, ranging from 0 to 70 degrees. One golden radial spoke was acquired per TR. Bottom: diagram of the proposed motion correction MRF (MC-MRF). 1) An iterative SENSE sliding window reconstruction is used to obtain intermediate temporally resolved images with reduced aliasing. 2) Intensity based rigid body image registration is used to estimate rotational and 2D translational motion. 3) Rigid motion correction is applied in k-space with the corresponding phase-shifts and rotations. 4) Low rank reconstruction of the motion corrected k-space is employed to produce the final time-points used for matching.

Figure 2: MRF simulations with no motion correction (NMC), image based motion correction (IBMC) and the proposed MC-MRF for abrupt rigid motion at time-point 250 (out of 1750 time-points). Motion towards the beginning of acquisition affects primarily $T_1$, but residual ghosting artefacts are also present in the $T_2$ and $M_0$ maps. MC-MRF reduces most motion artefacts and achieves similar image quality than the motion-free reference. IBMC also achieves good motion correction, however residual blurring artefacts are present. Estimated motion parameters for this simulation are shown in the corresponding Supplementary Figure 2.

Figure 3: MRF simulations with no motion correction (NMC), image based motion correction (IBMC) and the proposed MC-MRF for abrupt rigid motion at time-point 1500 (out of 1750 time-points). Motion towards the end of acquisition affects primarily $T_2$ (and $M_0$), but residual ghosting artefacts are also present in the $T_1$ map. MC-MRF reduces most motion artefacts and achieves similar image quality than the motion-free reference. IBMC also achieves good motion correction, however residual blurring artefacts are present. Estimated motion parameters for this simulation are shown in the corresponding Supplementary Figure 3.

Figure 4: MRF simulations with no motion correction (NMC), image based motion correction (IBMC) and the proposed MC-MRF for sinusoidally varying motion. All parametric maps are affected by continuous motion. MC-MRF reduces most motion artefacts and achieves similar

image quality than the motion-free reference. IBMC also achieves good motion correction, however residual blurring artefacts are present. Estimated motion parameters for this simulation are shown in the corresponding Supplementary Figure 4.

Figure 5: Results for a manually moved phantom experiment with predominant translational motion and minimal rotational motion. Considerable motion artefacts can be observed in both $T_1$ and $T_2$ maps in the case of no motion correction (NMC). These artefacts are greatly reduced with the proposed MC-MRF. Plots for the $T_1$ and $T_2$ values of the parametric phantom are shown below in comparison to gold standard values, where MC-MRF considerably improves the accuracy and precision of the measurements.

Figure 6: *In-vivo* results with in-plane motion for subjects 1 and 2 with no motion correction (NMC), motion corrected MRF (MC-MRF) and no motion. Ghosting and blurring artefacts propagate from the time-point images into the parametric maps in the NMC case. The proposed MC-MRF improves parametric map quality, to a comparable degree to the case of no motion. Doted blue areas in NMC $T_1$ for subject 1 denote the regions on interest used to measure white and grey matter parametric values. Estimated motion parameters for these subjects are shown in the Supplementary Figure 6.

Figure 7: *In-vivo* results with in-plane motion for subjects 3 and 4 with no motion correction (NMC), motion corrected MRF (MC-MRF) and no motion. Ghosting and blurring artefacts propagate from the time-point images into the parametric maps in the NMC case. The proposed MC-MRF improves parametric map quality, to a comparable degree to the case of no motion. Estimated motion parameters for these subjects are shown in the Supplementary Figure 6.

Figure 8: *In-vivo* results with through-plane motion for subjects 1 and 2 with no motion correction (NMC), motion corrected MRF (MC-MRF) and no motion. Considerable motion artefacts are present in NMC. Artefacts are reduced with the proposed MC-MRF, however residual errors remain in the parametric maps, especially in $T_2$.

Figure 9: *In-vivo* results with through-plane motion for subjects 3 and 4 with no motion correction (NMC), motion corrected MRF (MC-MRF) and no motion. Considerable motion artefacts are present in NMC. Artefacts are reduced with the proposed MC-MRF, however residual errors remain in the parametric maps, especially in $T_2$.

Table 1: $T_1$ and $T_2$ in healthy subjects for no motion correction (NMC), the proposed motion corrected MRF (MC-MRF) and the ground-truth (no motion).

Supporting Information Figure S1: Examples of time-point images for a low rank reconstruction with no motion correction (Non motion corrected) and intermediate time-points at different stages of the proposed framework: 1) Sliding window reconstruction, 2) Rigid registration and 4) (motion corrected) Low rank reconstruction.

Supporting Information Figure S2: Estimated motion parameters for the simulation experiment with abrupt rigid motion occurring at time-point 250, using image based motion correction (IBMC) and the proposed MC-MRF. Generally, both methods achieve accurate motion estimation, however higher errors are present for IBMC. Both methods present motion estimation errors around the abrupt motion discontinuities.

Supporting Information Figure S3: Estimated motion parameters for the simulation experiment with abrupt rigid motion occurring at time-point 1500, using image based motion correction (IBMC) and the proposed MC-MRF. Generally, both methods achieve accurate motion estimation, however higher errors are present for IBMC. Both methods present motion estimation errors around the abrupt motion discontinuities.

Supporting Information Figure S4: Estimated motion parameters for the simulation experiment with sinusoidally varying motion, using image based motion correction (IBMC) and the proposed MC-MRF. Generally, both methods achieve accurate motion estimation, however higher errors are present for IBMC.

Supporting Information Figure S5: Time-point images for subjects 1 and 2 with no motion correction (NMC) and the proposed motion corrected MRF (MC-MRF) from an acquisition with in-plane motion. In the presence of motion, low rank reconstruction with no motion correction introduces ghosting and blurring. MC-MRF greatly reduces motion artefacts, revealing image structures otherwise obscured.

Supporting Figure S6. Estimated rigid body motion in four representative brain subject *in-vivo* scans with in-plane motion. Rotational motion is shown in blue, left-right translation is shown in continuous red and anterior-posterior translation is shown in dashed red. The estimated motion captures the periodic nature of motion is subjects instructed to continuously move during the acquisition.

## References:

1. Ma D, Gulani V, Seiberlich N, Liu K, Sunshine JL, Duerk JL, Griswold MA. Magnetic resonance fingerprinting. Nature 2013;495:187–192.

2. Hennig J, Weigel M, Scheffler K. Calculation of flip angles for echo trains with predefined amplitudes with the extended phase graph (EPG)-algorithm: principles and applications to hyperecho and TRAPS sequences. Magn Reson 2004;51:68–80.

3. Weigel M. Extended phase graphs: Dephasing, RF pulses, and echoes - pure and simple. J Magn Reson Imaging 2015;41:266–295.

4. Pierre EY, Ma D, Chen Y, Badve C, Griswold MA. Multiscale reconstruction for MR fingerprinting. Magn Reson Med 2016;75:2481–2492.

5. Jiang Y, Ma D, Bhat H, Ye H, Cauley SF, Wald LL, Setsompop K, Griswold MA. Use of pattern recognition for unaliasing simultaneously acquired slices in simultaneous multislice MR fingerprinting. Magn Reson Med doi:10.1002/mrm.26572.

6. Cao X, Liao C, Wang Z, Chen Y, Ye H, He H, Zhong J. Robust sliding-window reconstruction for Accelerating the acquisition of MR fingerprinting. Magn Reson Med doi:10.1002/mrm.26521.

7. Cruz G, Gaspar AS, Bruijnen T, Botnar RM, Prieto C. Accelerated Magnetic Resonance Fingerprinting using Soft-weighted key-Hole (MRF-SOHO). Proceedings of the 23rd scientific meeting, International Society for Magnetic Resonance in Medicine, Honolulu, p 135.

8. McGivney DF, Pierre E, Ma D, Jiang Y, Saybasili H, Gulani V, Griswold MA. SVD compression for magnetic resonance fingerprinting in the time domain. IEEE Trans Med Imaging 2014;33(12):2311-22.

9. Doneva M, Amthor T, Koken P, Sommer K, Börnert P. Matrix completion-based reconstruction for undersampled magnetic resonance fingerprinting data. Magn Reson Imaging http://doi.org/10.1016/j.mri.2017.02.007

10. Zhao B, Setsompop K, Adalsteinsson E, Gagoski B, Ye H, Ma D, Jiang Y, Ellen Grant P, Griswold MA, Wald LL. Improved magnetic resonance fingerprinting reconstruction with low-rank and subspace modelling. Magn Reson Med 2017. doi: 10.1002/mrm.26701

11. Assländer J, Cloos MA, Knoll F, Sodickson DK, Hennig J, Lattanzi R. Low Rank Alternating Direction Method of Multipliers Reconstruction for MR Fingerprinting. Magn Reson Med 2017. doi:10.1002/mrm.26639

12. Zhao B. Model-based iterative reconstruction for magnetic resonance fingerprinting. InImage Processing (ICIP) 2015 IEEE International Conference 2015 (pp. 3392-3396). IEEE.

13. G. Mazor, L. Weizman, A. Tal and Y. C. Eldar, "Low rank magnetic resonance fingerprinting," 38th Annual International Conference of the IEEE Engineering in Medicine and Biology Society 2016. doi: 10.1109/EMBC.2016.7590734

14. Otazo R, Candès E, Sodickson DK. Low‐rank plus sparse matrix decomposition for accelerated dynamic MRI with separation of background and dynamic components. Magnetic Resonance in Medicine 2015;73(3):1125-36.

15. Weizman L, Miller KL, Eldar YC, Chiew M. PEAR: PEriodic And fixed Rank separation for fast fMRI. Med Phys 2017;44(12):6166-82.

16. Lingala SG, Hu Y, DiBella E, Jacob M. Accelerated dynamic MRI exploiting sparsity and low-rank structure: kt SLR. IEEE Trans Med Imag 2011;30(5):1042-54.

17. Zhao B, Haldar JP, Brinegar C, Liang ZP. Low rank matrix recovery for real-time cardiac MRI. InBiomedical Imaging: From Nano to Macro, IEEE International Symposium 2010 (pp. 996-999).

18. Boyd S, Parikh NE, Chu BP, Eckstein J. Distributed optimization and statistical learning via the alternating direction method of multipliers. Found Trends Mach Learn 2011;3:1–122.

19. Chen Y, Jiang Y, Pahwa S, Ma D, Lu L, Twieg MD, Wright KL, Seiberlich N, Griswold MA, Gulani V. MR fingerprinting for rapid quantitative abdominal imaging. Radiology 2016;279:278–286.

20. Hamilton JI, Jiang Y, Chen Y, Ma D, Lo WC, Griswold MA, Seiberlich N. MR fingerprinting for rapid quantification of myocardial $T_1$, $T_2$, and proton spin density. Magn Reson Med doi:10.1002/mrm.26216.

21. Pipe JG. Motion correction with PROPELLER MRI: application to head motion and free-breathing cardiac imaging. Magn Reson Med 1999;42(5):963-9.

22. Graedel NN, McNab JA, Chiew M, Miller KL. Motion correction for functional MRI with three‐dimensional hybrid radial‐Cartesian EPI. Magn Reson Med 2017;78(2):527-40.

23. Mehta BB, Ma D, Coppo S, Griswold MA. Image Reconstruction Algorithm for Motion Insensitive Magnetic Resonance Fingerprinting (MRF). Proceedings of the 23rd scientific meeting, International Society for Magnetic Resonance in Medicine, Honolulu, p 302.

24. Xu Z, Lyu M, Hui E, Mei Y, Chen Z, Chen W, Xu EX, Feng Y. Motion Correction for Magnetic Resonance Fingerprinting by Using Sliding-Window Reconstruction and Image Registration. Proceedings of the 23rd scientific meeting, International Society for Magnetic Resonance in Medicine, Honolulu, p 1273.

25. Cruz G, Botnar RM, Prieto C. Motion corrected Magnetic Resonance Fingerprinting using Soft-weighted key-Hole (MRF-McSOHO). Proceedings of the 23rd scientific meeting, International Society for Magnetic Resonance in Medicine, Honolulu, p 935.

26. Yu Z, Zhao T, Asslander J, Lattanzi R, Sodickson DK, Cloos MA. Exploring the Sensitivity of Magnetic Resonance Fingerprinting to Different Types of Motion and Possible

Correction Mechanisms. Proceedings of the 23rd scientific meeting, International Society for Magnetic Resonance in Medicine, Honolulu, p 3938.

27. Anderson CE, Wang CY, Gu Y, Darrah R, Griswold MA, Yu X, Flask CA. Regularly incremented phase encoding – MR fingerprinting (RIPE-MRF) for enhanced motion artifact suppression in preclinical cartesian MR fingerprinting. Magn Reson Med 2017; doi: 10.1002/mrm.26865

28. Pruessmann KP, Weiger M, Börnert P, Boesiger P. Advances in sensitivity encoding with arbitrary k-space trajectories. Magn Reson Med 2001;46:638–651.

29. Jiang Y, Ma D, Seiberlich N, Gulani V, Griswold MA. MR fingerprinting using fast imaging with steady state precession (FISP) with spiral readout. Magn Reson Med 2015;74:1621–1631.

30. Captur G, Gatehouse P, Kellman P, Heslinga FG, Keenan K, Bruehl R, Prothmann M, Graves MJ, Chiribiri A, Ittermann B, Pang W, Nezafat R, Salerno M, Moon JC. A T1 and ECV phantom for global T1 mapping quality assurance: The T1 mapping and ECV standardisation in CMR (T1MES) program. J Cardiov Magn Reson 2016;18(1):1.

31. Winkelmann S, Schaeffter T, Koehler T, Eggers H, Doessel O. An optimal radial profile order based on the Golden Ratio for time-resolved MRI. IEEE T Med Imaging 2007;26(1):68-76.

32. Uecker M, Lai P, Murphy MJ, Virtue P, Elad M, Pauly JM, Vasanawala SS, Lustig M. ESPIRiT—an eigenvalue approach to autocalibrating parallel MRI: Where SENSE meets GRAPPA. Magn Reson Med 2014;71:990–1001.

33. Rasche V, Proksa R, Sinkus R, Bornert P, Eggers H. Resampling of data between arbitrary grids using convolution interpolation. IEEE T Med Imaging 1999;18(5):385-392.

34. Greengard L, Lee JY. Accelerating the Nonuniform Fast Fourier Transform. SIAM Review 2004;46(3):443-454.

35. Ma D, Coppo S, Chen Y, McGivney DF, Jiang Y, Pahwa S, Gulani V, Griswold MA. Slice profile and B1 corrections in 2D magnetic resonance fingerprinting. Magn Reson Med doi:10.1002/mrm.26580

36. Assländer J, Glaser SJ, Hennig J. Pseudo Steady-State Free Precession for MR-Fingerprinting. Magn Reson Med 2017;77: 1151–1161. doi: 10.1002/mrm.26202

37. Maclaren J, Herbst M, Speck O, Zaitsev M. Prospective motion correction in brain imaging: a review. Magn Reson Med 2013;69(3):621-36.

38. Stehning C, Börnet P, Nehrke K, Eggers H, Dössel O. Fast isotropic volumetric coronary MR angiography using free-breathing 3D radial balanced FFE acquisition. Magn Reson Med 2004; 52: 197–203

39. Piccini D, Littmann A, Nielles-Vallespin S, Zenge M. Spiral phyllotaxis: the natural way to construct a 3D Radial trajectory in MRI. Magn Reson Med. 2011;66:1049–1056.

40. Lustig M, Donoho D, Pauly JM. Sparse MRI: the application of compressed sensing for rapid MR imaging. Magn Reson Med 2007;58:1182–1195.

41. Atkinson D, Hill DLG, Stoyle PNR, Summers PE, Clare S, Bowtell R, Keevil SF. Automatic compensation of motion artifacts in MRI. Magn Reson Med 1999;41:163–170.

42. Batchelor PG, Atkinson D, Irarrazaval P, Hill DLG, Hajnal J, Larkman D. Matrix description of general motion correction applied to multishot images. Magn Reson Med 2005;54:1273–1280.

43. Cheng JY, Alley MT, Cunningham CH, Vasanawala SS, Pauly JM, Lustig M. Nonrigid motion correction in 3D using autofocusing with localized linear translations. Magn Reson Med 2012;68:1785–1797.

44. Buonincontri G, Sawiak SJ. MR fingerprinting with simultaneous B1 estimation. Magn Reson Med 2016;76:1127–1135.

45. Hilbert T, Kober T, Zhao T, Block TK, Yu Z, Thiran JP, Krueger G, Sodickson DK, Cloos M. Mitigating the effect of magnetization transfer in magnetic resonance fingerprinting. Proceedings of the 23rd scientific meeting, International Society for Magnetic Resonance in Medicine, Honolulu, p 74.

46. Ma D, Jiang Y, Chen Y, McGivney D, Mehta B, Gulani V,Griswold M. Fast 3D magnetic resonance fingerprinting for a whole-brain coverage. Magn Reson Med 2017 doi: 10.1002/mrm.2688.

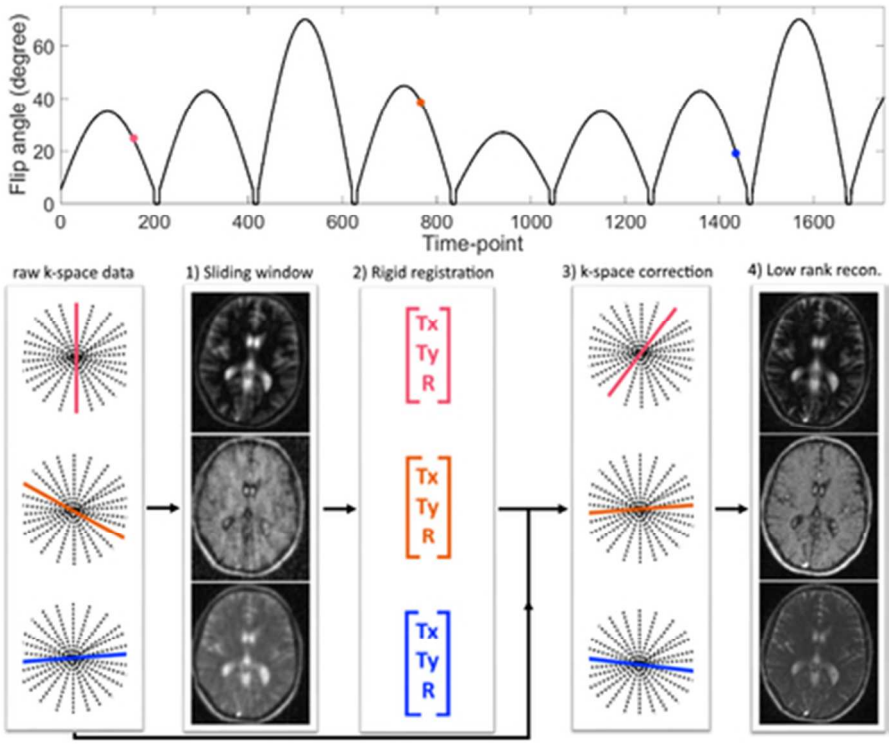


Figure 1. Top: plot of the flip angle pattern used for all experiments, ranging from 0 to 70 degrees. One golden radial spoke was acquired per TR. Bottom: diagram of the proposed motion correction MRF (MC-MRF). 1) An iterative SENSE sliding window reconstruction is used to obtain intermediate temporally resolved images with reduced aliasing. 2) Intensity based rigid body image registration is used to estimate rotational and 2D translational motion. 3) Rigid motion correction is applied in k-space with the corresponding phase-shifts and rotations. 4) Low rank reconstruction of the motion corrected k-space is employed to produce the final time-points used for matching.

18x15mm (600 x 600 DPI)

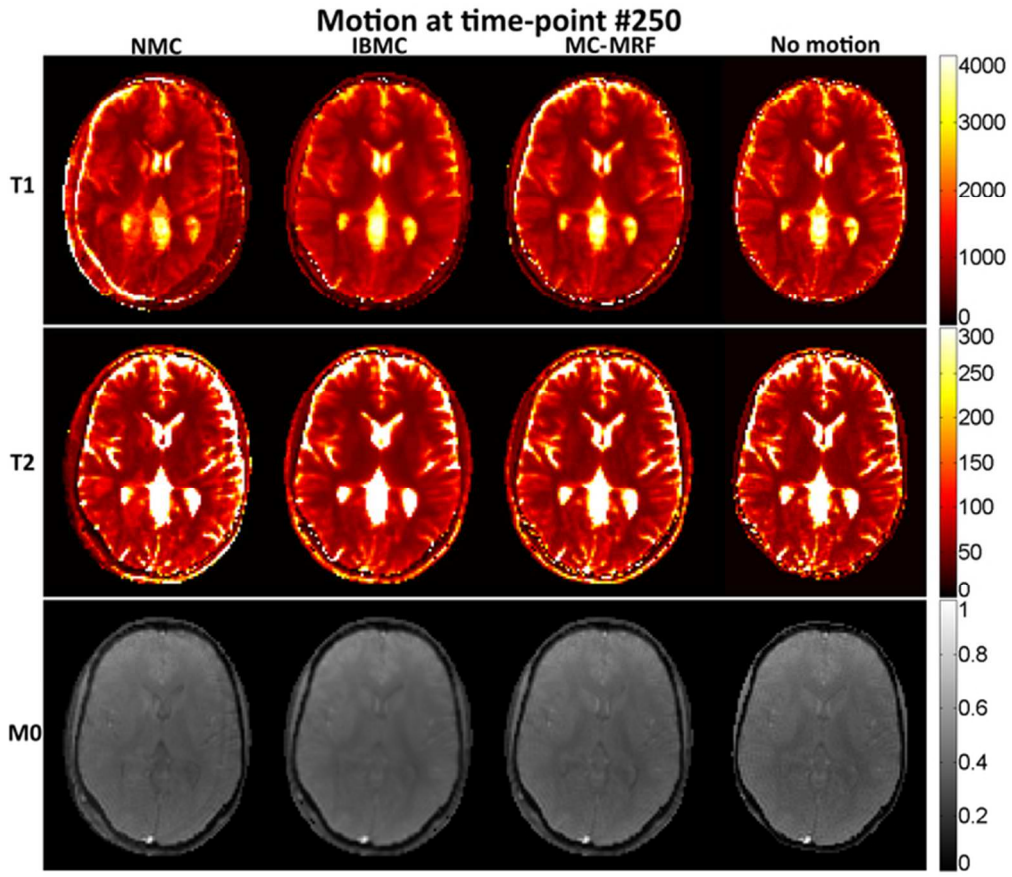


Figure 2: MRF simulations with no motion correction (NMC), image based motion correction (IBMC) and the proposed MC-MRF for abrupt rigid motion at time-point 250 (out of 1750 time-points). Motion towards the beginning of acquisition affects primarily T1, but residual ghosting artefacts are also present in the T2 and M0 maps. MC-MRF reduces most motion artefacts and achieves similar image quality than the motion-free reference. IBMC also achieves good motion correction, however residual blurring artefacts are present. Estimated motion parameters for this simulation are shown in the corresponding Supplementary Figure 2.

29x25mm (600 x 600 DPI)

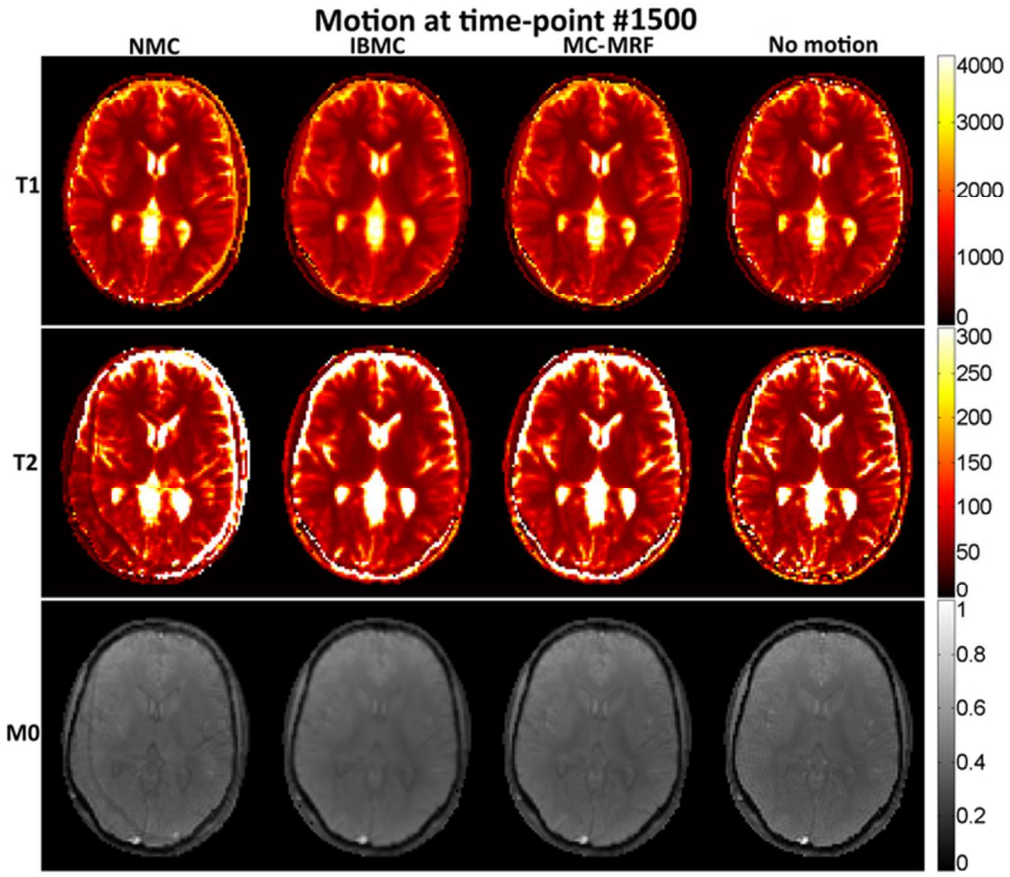


Figure 3: MRF simulations with no motion correction (NMC), image based motion correction (IBMC) and the proposed MC-MRF for abrupt rigid motion at time-point 1500 (out of 1750 time-points). Motion towards the end of acquisition affects primarily T2 (and M0), but residual ghosting artefacts are also present in the T1 map. MC-MRF reduces most motion artefacts and achieves similar image quality than the motion-free reference. IBMC also achieves good motion correction, however residual blurring artefacts are present. Estimated motion parameters for this simulation are shown in the corresponding Supplementary Figure 3.

29x25mm (600 x 600 DPI)

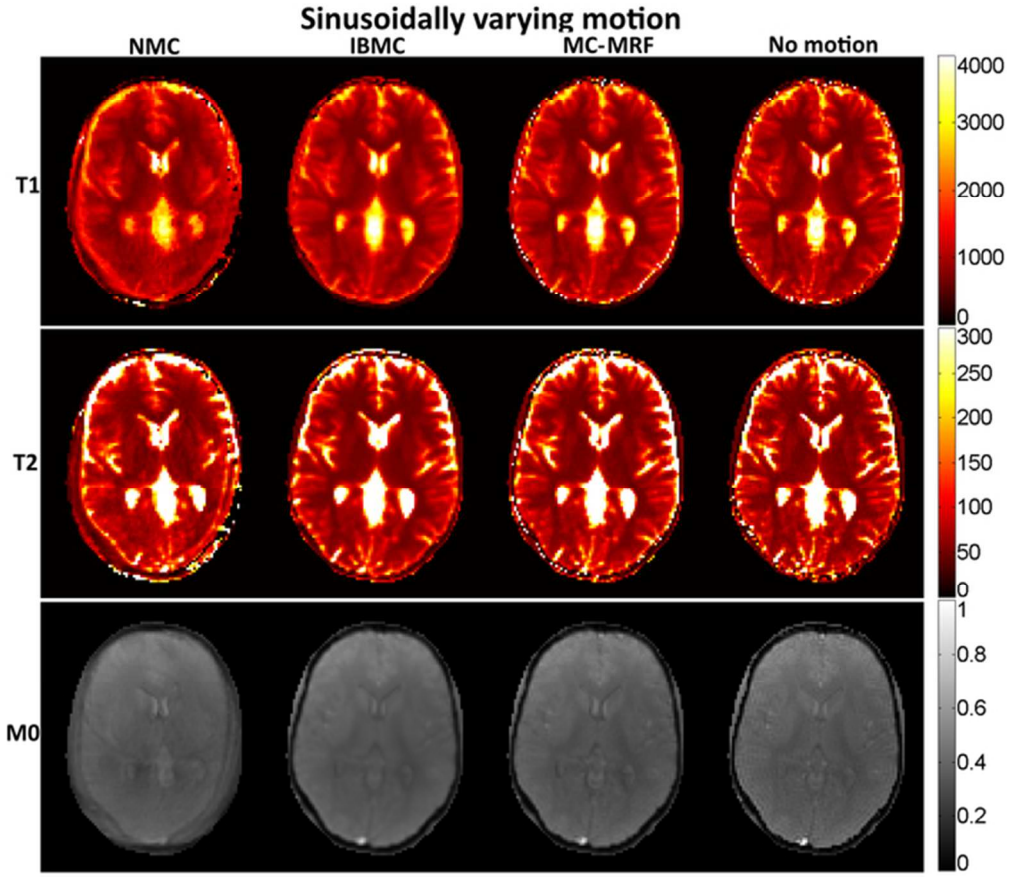


Figure 4: MRF simulations with no motion correction (NMC), image based motion correction (IBMC) and the proposed MC-MRF for sinusoidally varying motion. All parametric maps are affected by continuous motion. MC-MRF reduces most motion artefacts and achieves similar image quality than the motion-free reference. IBMC also achieves good motion correction, however residual blurring artefacts are present. Estimated motion parameters for this simulation are shown in the corresponding Supplementary Figure 4.

29x25mm (600 x 600 DPI)

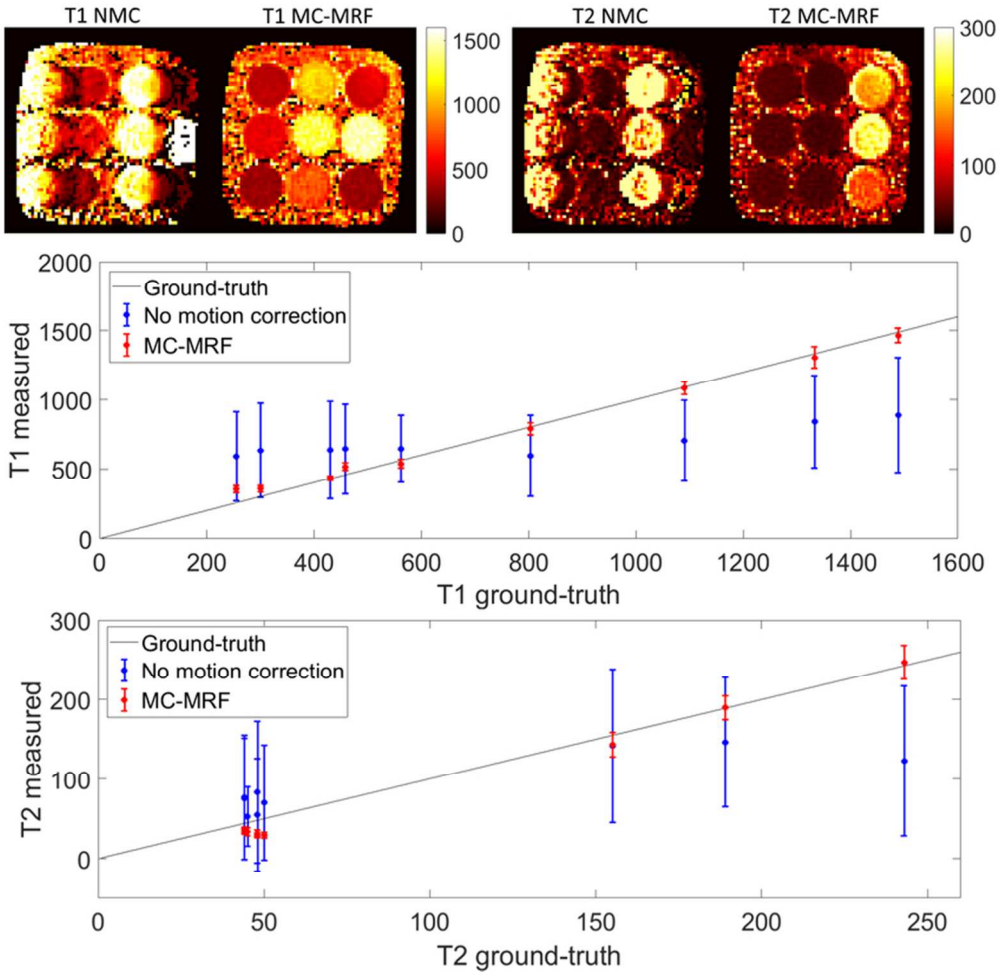


Figure 5: Results for a manually moved phantom experiment with predominant translational motion and minimal rotational motion. Considerable motion artefacts can be observed in both T1 and T2 maps in the case of no motion correction (NMC). These artefacts are greatly reduced with the proposed MC-MRF. Plots for the T1 and T2 values of the parametric phantom are shown below in comparison to gold standard values, where MC-MRF considerably improves the accuracy and precision of the measurements.

35x35mm (600 x 600 DPI)

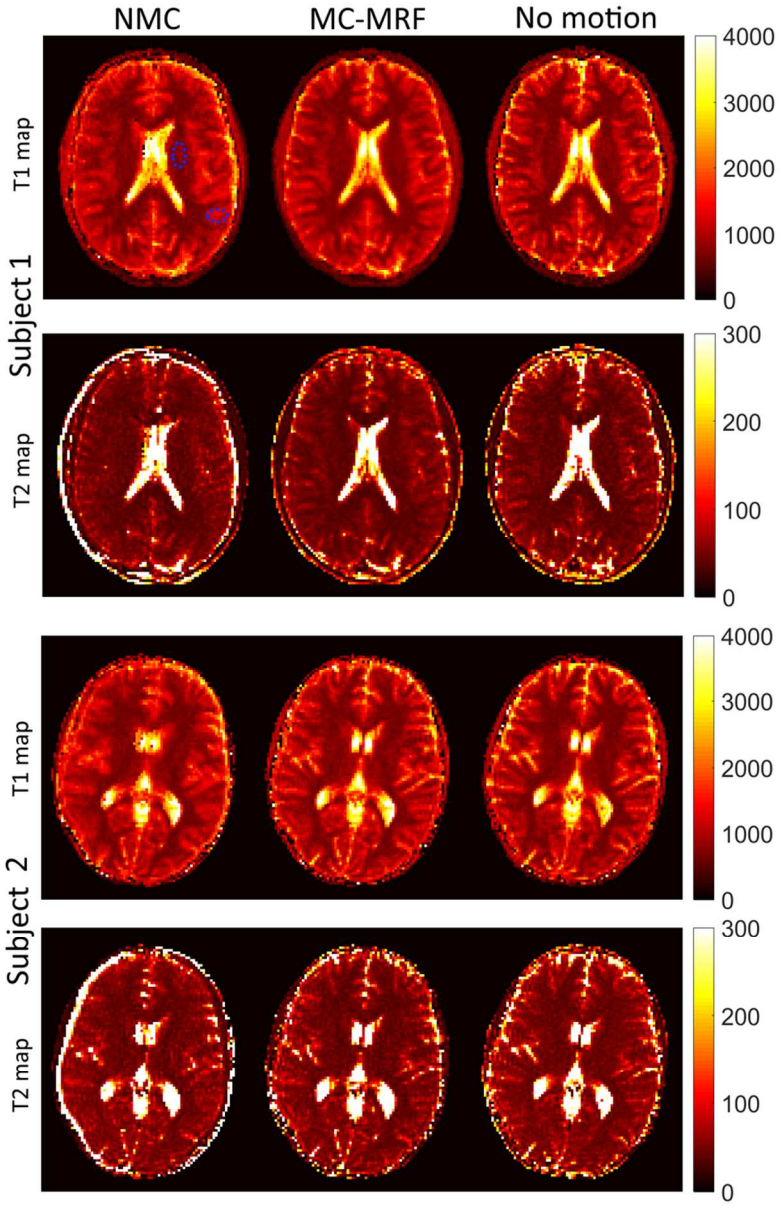


Figure 6: In-vivo results with in-plane motion for subjects 1 and 2 with no motion correction (NMC), motion corrected MRF (MC-MRF) and no motion. Ghosting and blurring artefacts propagate from the time-point images into the parametric maps in the NMC case. The proposed MC-MRF improves parametric map quality, to a comparable degree to the case of no motion. Doted blue areas in NMC T1 for subject 1 denote the regions on interest used to measure white and grey matter parametric values. Estimated motion parameters for these subjects are shown in the Supplementary Figure 6.

40x62mm (600 x 600 DPI)

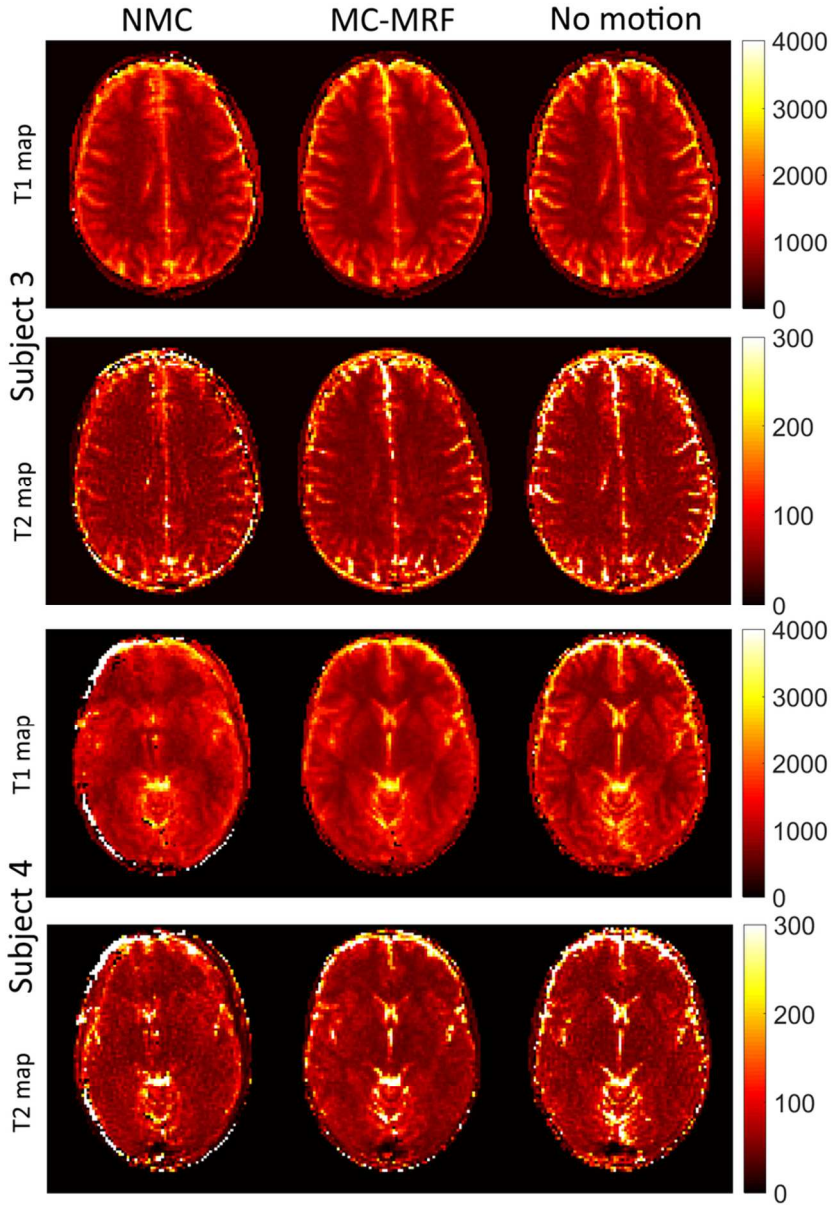


Figure 7: In-vivo results with in-plane motion for subjects 3 and 4 with no motion correction (NMC), motion corrected MRF (MC-MRF) and no motion. Ghosting and blurring artefacts propagate from the time-point images into the parametric maps in the NMC case. The proposed MC-MRF improves parametric map quality, to a comparable degree to the case of no motion. Estimated motion parameters for these subjects are shown in the Supplementary Figure 6.

38x55mm (600 x 600 DPI)

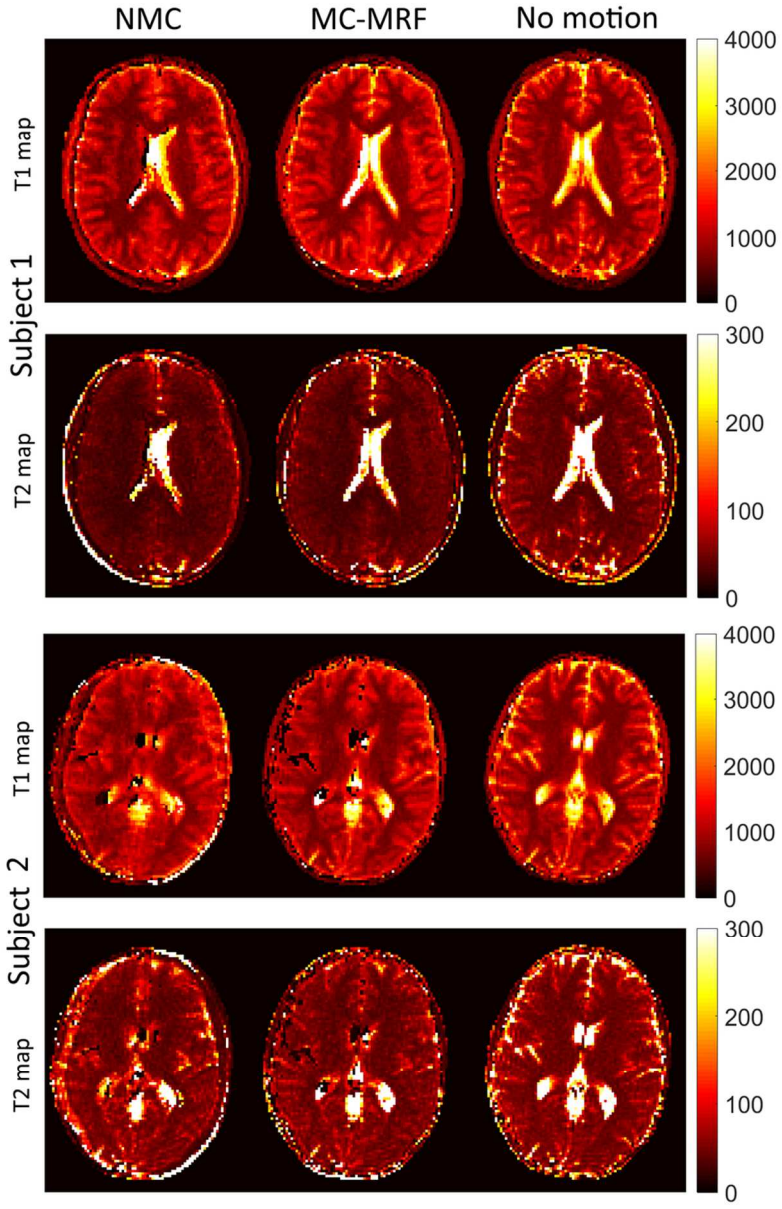


Figure 8: In-vivo results with through-plane motion for subjects 1 and 2 with no motion correction (NMC), motion corrected MRF (MC-MRF) and no motion. Considerable motion artefacts are present in NMC. Artefacts are reduced with the proposed MC-MRF, however residual errors remain in the parametric maps, especially in T2.

40x62mm (600 x 600 DPI)

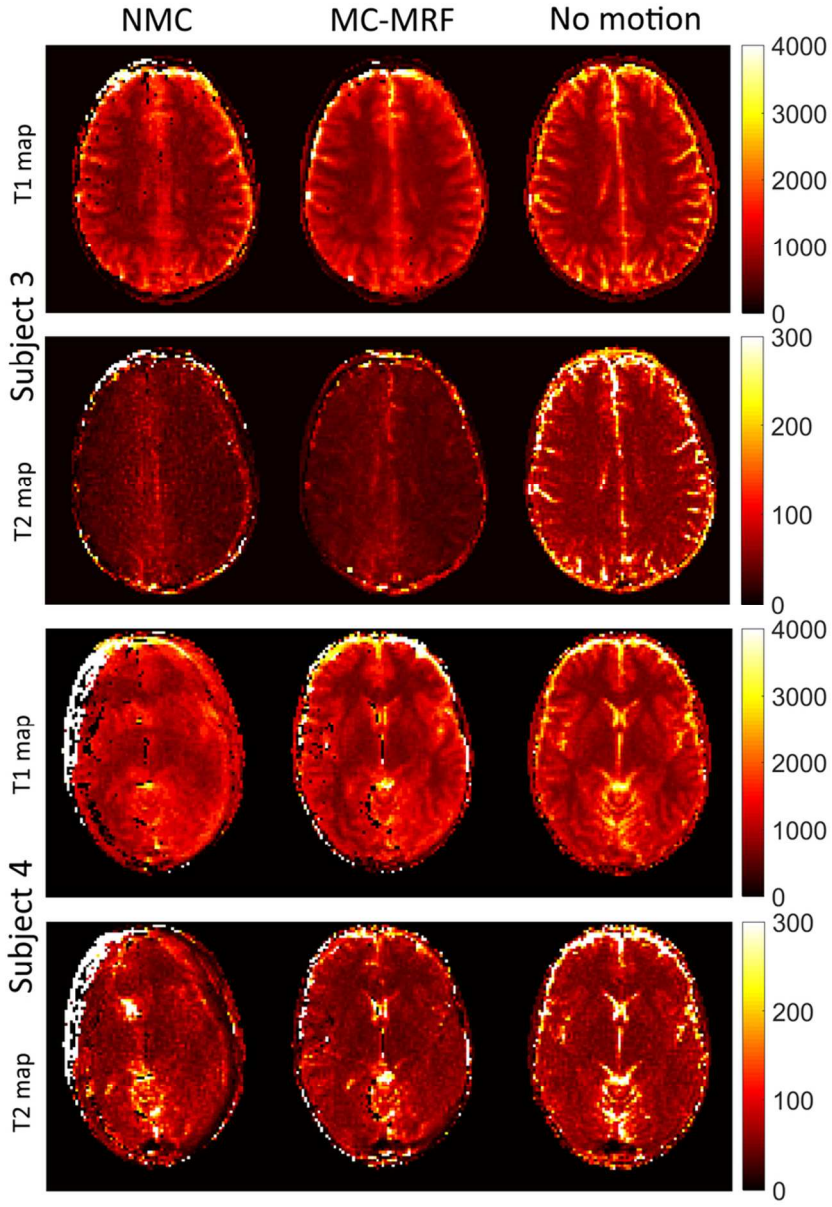


Figure 9: In-vivo results with through-plane motion for subjects 3 and 4 with no motion correction (NMC), motion corrected MRF (MC-MRF) and no motion. Considerable motion artefacts are present in NMC. Artefacts are reduced with the proposed MC-MRF, however residual errors remain in the parametric maps, especially in T2.

38x55mm (600 x 600 DPI)

Table 1: $T_1$ and $T_2$ in healthy subjects for no motion correction (NMC), the proposed motion corrected MRF (MC-MRF) and the ground-truth (no motion).

| | In-plane NMC | In-plane MC-MRF | Through-plane NMC | Through-plane MC-MRF | No motion | Literature |
|---|---|---|---|---|---|---|
| T1 white matter | 753 ± 33 | 743 ± 32 | 769 ± 58 | 721 ± 47 | 738 ± 20 | 608-756 |
| T2 white matter | 49 ± 6 | 47 ± 5 | 41 ± 7 | 39 ± 6 | 48 ± 5 | 54-81 |
| T1 grey matter | 1074 ± 22 | 1159 ± 29 | 1069 ± 64 | 1104 ± 61 | 1127 ± 28 | 998-1304 |
| T2 grey matter | 63 ± 5 | 63 ± 4 | 47 ± 9 | 47 ± 9 | 69 ± 5 | 78-98 |

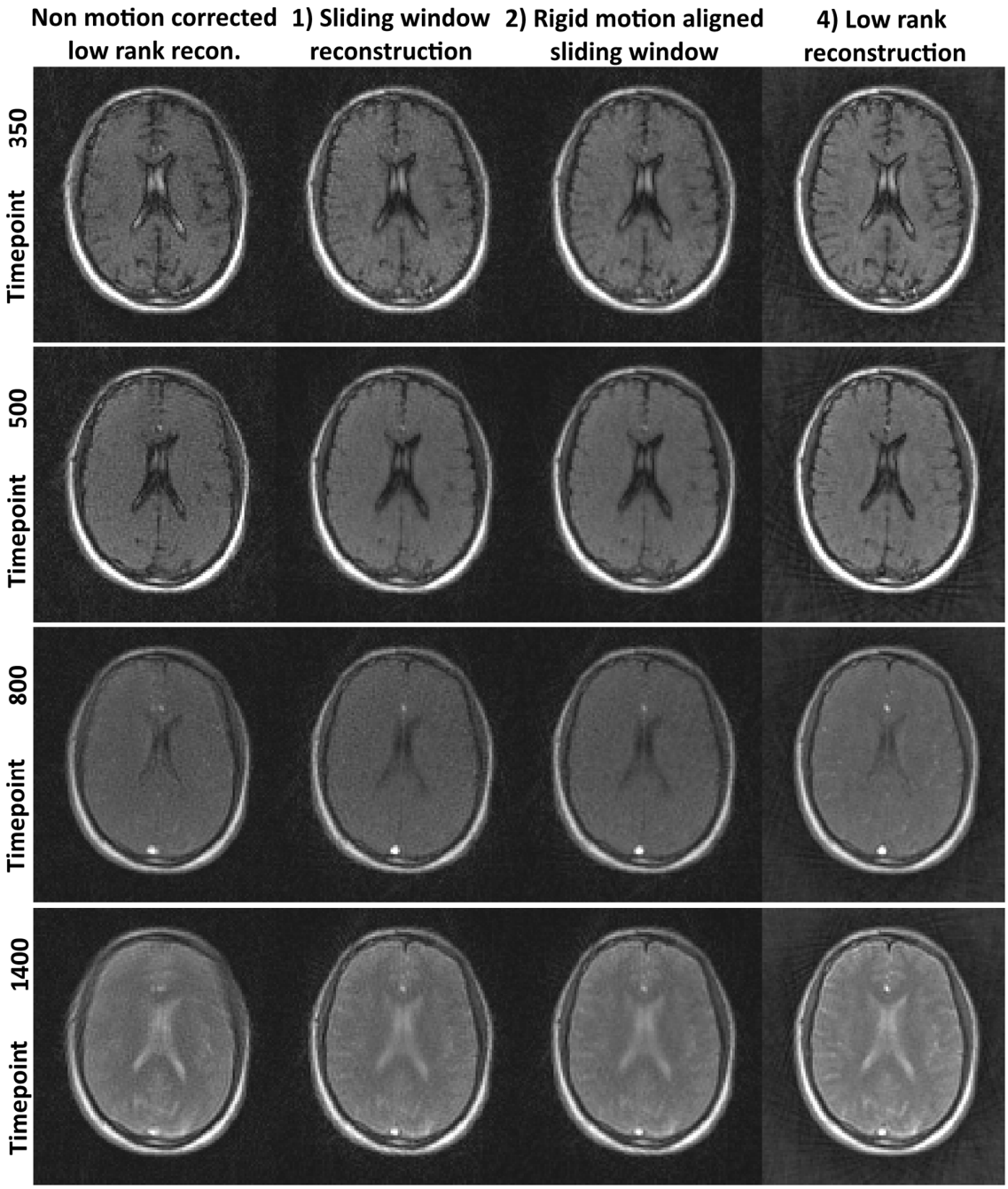


Supporting Information Figure S1: Examples of time-point images for a low rank reconstruction with no motion correction (Non motion corrected) and intermediate time-points at different stages of the proposed framework: 1) Sliding window reconstruction, 2) Rigid registration and 4) (motion corrected) Low rank reconstruction.

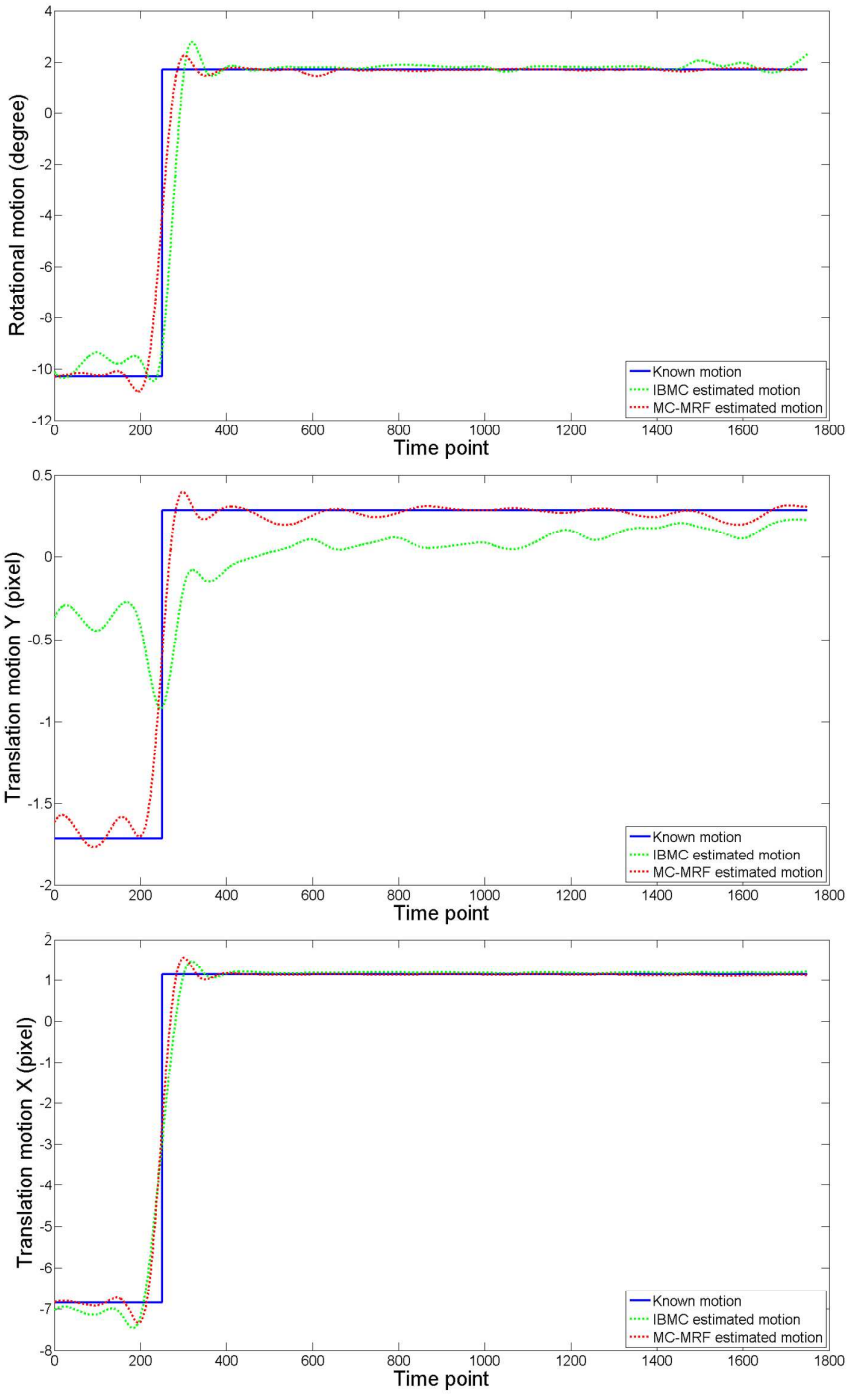


Supporting Information Figure S2: Estimated motion parameters for the simulation experiment with abrupt rigid motion occurring at time-point 250, using image based motion correction (IBMC) and the proposed MC-MRF. Generally, both methods achieve accurate motion estimation, however higher errors are present for IBMC. Both methods present motion estimation errors around the abrupt motion discontinuities.

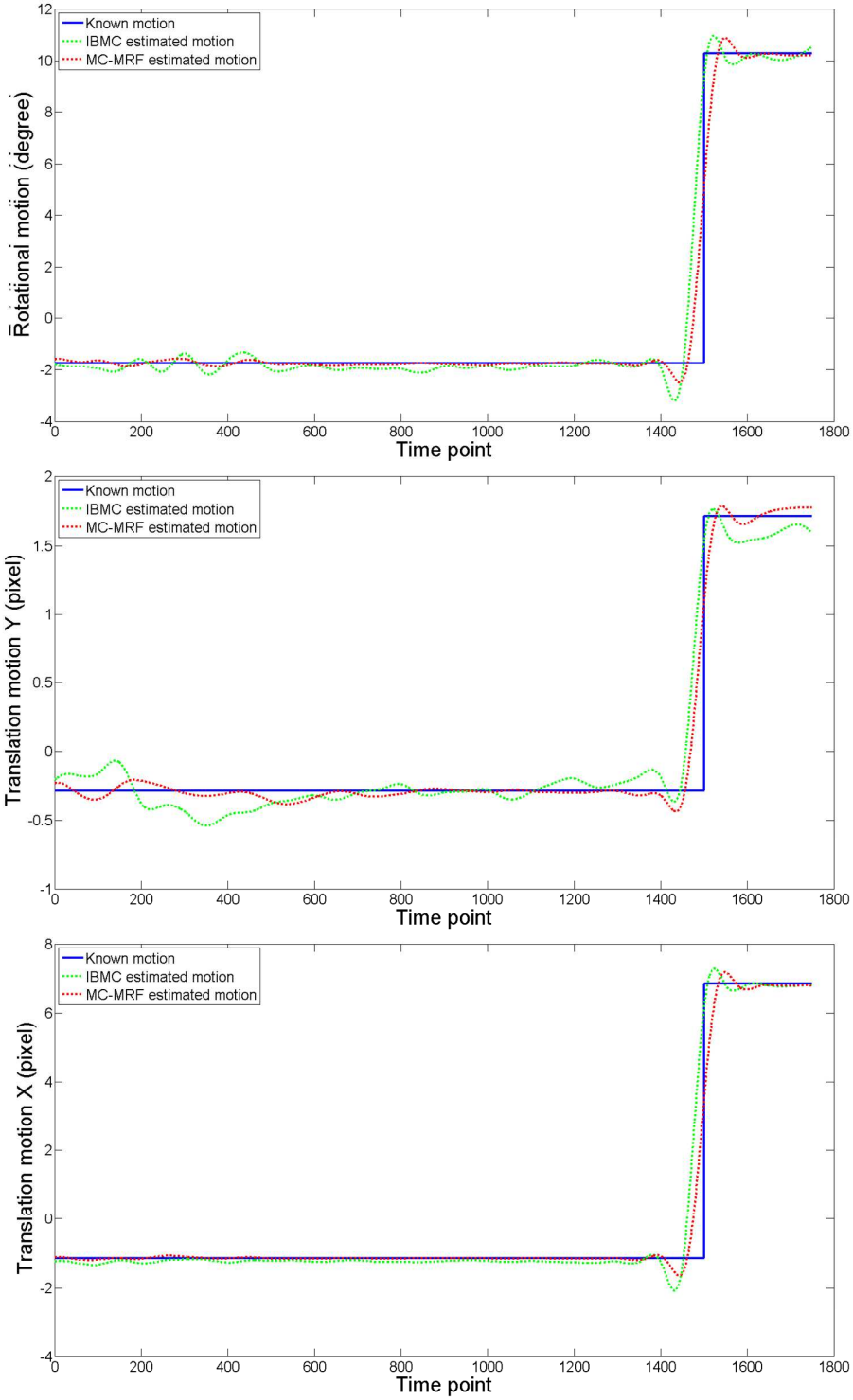


Supporting Information Figure S3: Estimated motion parameters for the simulation experiment with abrupt rigid motion occurring at time-point 1500, using image based motion correction (IBMC) and the proposed MC-MRF. Generally, both methods achieve accurate motion estimation, however higher errors are present for IBMC. Both methods present motion estimation errors around the abrupt motion discontinuities.

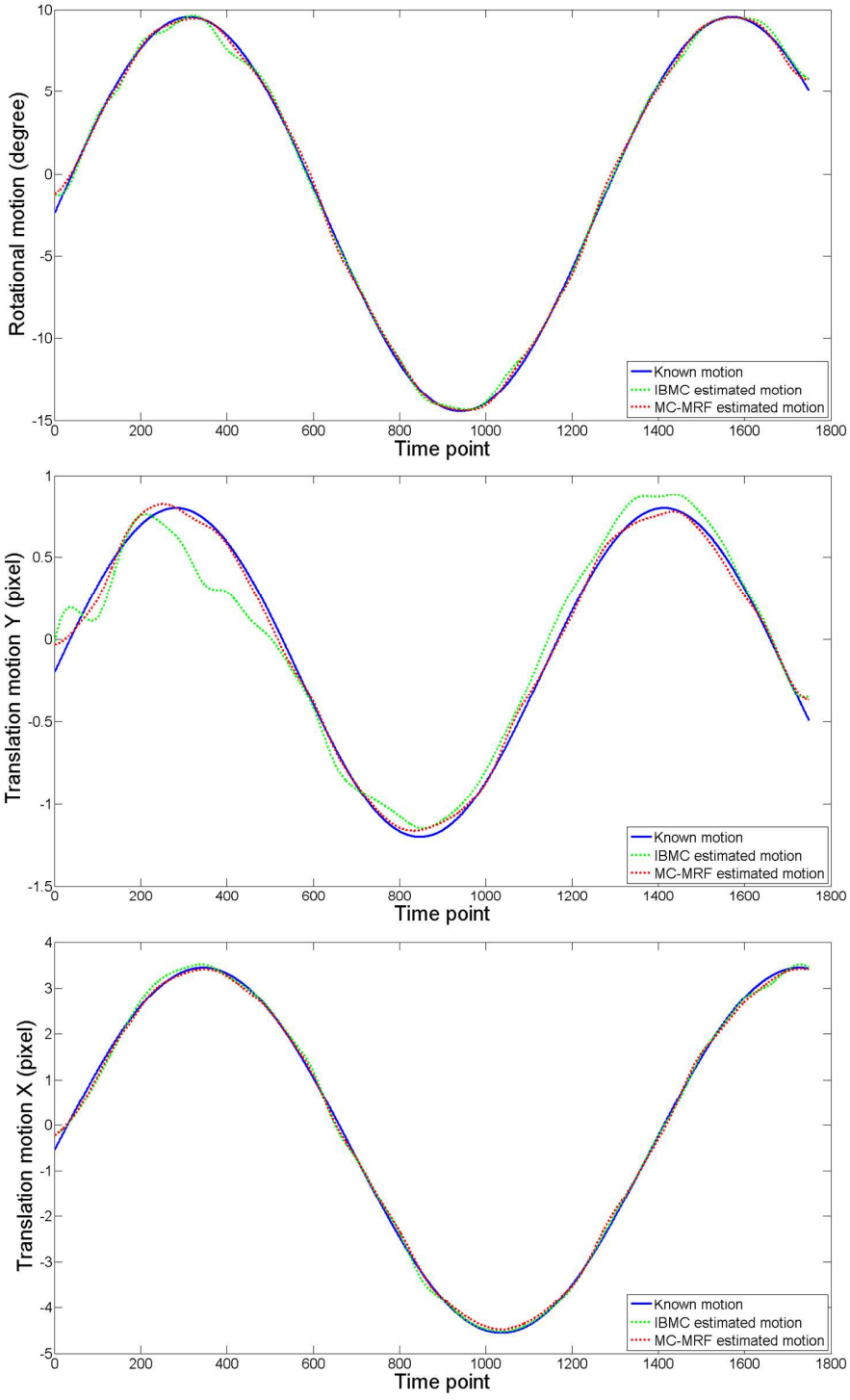


Supporting Information Figure S4: Estimated motion parameters for the simulation experiment with sinusoidally varying motion, using image based motion correction (IBMC) and the proposed MC-MRF. Generally, both methods achieve accurate motion estimation, however higher errors are present for IBMC.

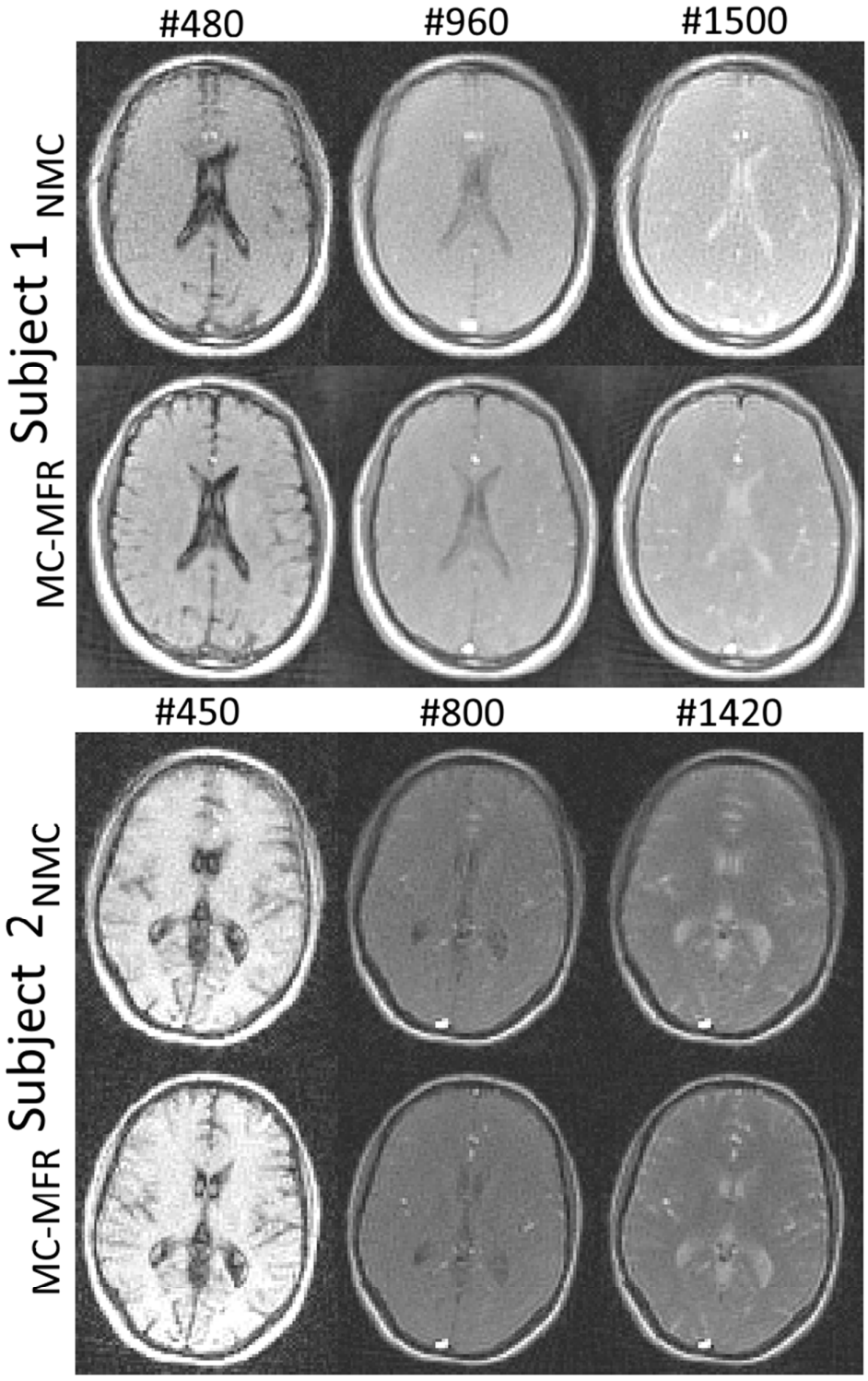


Supporting Information Figure S5: Time-point images for two different subjects with no motion correction (NMC) and the proposed motion corrected MRF (MC-MRF) from an acquisition with in-plane motion. In the presence of motion, low rank reconstruction with no motion correction introduces ghosting and blurring. MC-MRF greatly reduces motion artefacts, revealing image structures otherwise obscured.

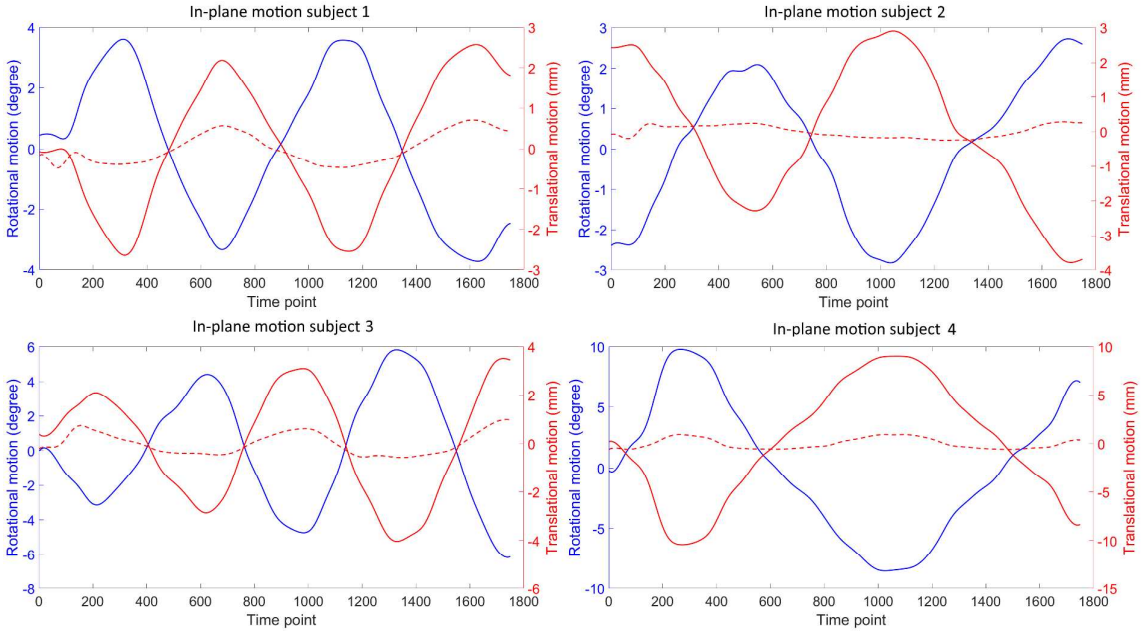


Supporting Information Figure S6. Estimated rigid body motion in four representative brain subject *in-vivo* scans with in-plane motion. Rotational motion is shown in blue, left-right translation is shown in continuous red and anterior-posterior translation is shown in dashed red. The estimated motion captures the periodic nature of motion is subjects instructed to continuously move during the acquisition. Note different motion amplitudes performed by different subjects.